NeuroImage 125 (2016) 256–266

Contents lists available at ScienceDirect

NeuroImage

journal homepage: www.elsevier.com/locate/ynimg

Structural and functional neuroplasticity in human learning of spatial routes

Timothy A. Keller *, Marcel Adam Just

Center for Cognitive Brain Imaging, Department of Psychology, Carnegie Mellon University, Pittsburgh, PA, USA

ARTICLE INFO

Article history:
Received 27 May 2015
Accepted 6 October 2015
Available online 20 October 2015

Keywords:
Spatial learning
Neuroplasticity
Connectivity
Hippocampus
Precuneus
fMRI
DTI

ABSTRACT

Recent findings with both animals and humans suggest that decreases in microscopic movements of water in the hippocampus reflect short-term neuroplasticity resulting from learning. Here we examine whether such neuroplastic structural changes concurrently alter the functional connectivity between hippocampus and other regions involved in learning. We collected both diffusion-weighted images and fMRI data before and after humans performed a 45 min spatial route-learning task. Relative to a control group with equal practice time, there was decreased diffusivity in the posterior-dorsal dentate gyrus of the left hippocampus in the route-learning group accompanied by increased synchronization of fMRI-measured BOLD signal between this region and cortical areas, and by changes in behavioral performance. These concurrent changes characterize the multi-dimensionality of neuroplasticity as it enables human spatial learning.

Introduction

The ability of the central nervous system to learn from experience and adapt to the environment is undeniably the result of its remarkable capacity for structural and functional change. The term *neuroplasticity* refers to a wide range of such changes, both anatomical and physiological, and it is studied at multiple levels and units of analysis. Neuroplastic mechanisms include changes at molecular, biochemical, synaptic, dendritic, axonal, morphological, and conectonomic levels. Part of the challenge of understanding neuroplasticity lies in relating its multiple facets to each other.

Although neuroplasticity has been studied in animals for over half a century by examining both anatomical (Diamond et al., 1964) and physiological (Zhang and Sejnowski, 2000) changes related to experience, only recently has neuroimaging allowed neuroplasticity to be investigated in vivo in humans. High-resolution structural images of the living human brain enabled precise measurement of changes in tissue volume longitudinally. Early correlational evidence showed that macroscopic morphological changes could be detected with MRI. For example, the posterior hippocampi of London taxi drivers with extensive navigation experience were larger than those of control participants (Maguire et al., 2000). Draganski et al. provided some of the first longitudinal evidence of learning-induced structural plasticity in humans by showing voxel-based morphometric changes in the gray matter of bilateral temporal visual motion areas and the left intraparietal sulcus following three months of training on juggling (Draganski et al., 2004). Additional studies of gray matter have suggested neuroplastic changes resulting from intensive training or learning in domains such as medical knowledge (Draganski et al., 2006), spatial memory (Maguire et al., 2006; Woollett and Maguire, 2011), and aerobic exercise (Colcombe et al., 2006; Erickson et al., 2011).

Another MRI-based structural imaging technique, diffusion-weighted imaging, also provides evidence of neuroplascticity resulting from intensive training and/or learning. Keller & Just showed that approximately 100 h of intensive reading remediation led to increased fractional anisotropy (FA) in the left frontal lobe, and that this change was correlated with changes in reading ability among children (Keller and Just, 2009). Sholz et al. found that six weeks of juggling training in adults resulted in FA increases in the white matter beneath the right intraparietal sulcus (Scholz et al., 2009). Additional studies now suggest adult FA increases following balance training (Taubert et al., 2010), working memory training in aging participants (Lövdén et al., 2010; Engvig et al., 2011), and meditation training (Tang et al., 2010). A number of reviews and critiques of both the gray matter and white matter changes resulting from relatively long-term, intensive learning or training regimens in adults have recently appeared (Zatorre et al., 2012; Lövdén et al., 2013).

Although these human in vivo experimental studies of neuroplasticity have involved extensive training, and have examined rather macroscopic structural changes, it is clear that learning-related changes in the brain must occur over shorter intervals and at more microscopic levels (Fu and Zuo, 2011). The cellular bases of experience-based structural changes

* Corresponding author at: Center for Cognitive Brain Imaging, Department of Psychology, Carnegie Mellon University, 5000 Forbes Ave., Pittsburgh, PA 15213, USA. Fax: +1 412 268 2804.
E-mail address: tk37@andrew.cmu.edu (T.A. Keller).

http://dx.doi.org/10.1016/j.neuroimage.2015.10.015
1053-8119/

in both gray and white matter remain speculative, but in a pioneering study that related structural and cellular changes, Blumenfeld-Katzir et al. demonstrated that diffusion imaging can detect neuroplastic changes in gray matter (Blumenfeld-Katzir et al., 2011). Following long-term training (a week) on a spatial-learning water maze task, rats showed decreases in diffusivity of water in the hippocampus and increases in quantitative cellular-level markers for synapses and astrocytes.

These findings of neuroplasticity have been extended to humans and to shorter training episodes in a series of recent papers from the same laboratory (Sagi et al., 2012; Hofstetter et al., 2013; Tavor et al., 2013). Sagi et al. trained both rats and humans on a spatial route-learning task for 2 h, comparing diffusion-weighted imaging before and after the training. The human participants engaged in a video-game driving task where they practiced driving the same route repeatedly. Compared to a control group that practiced on many different routes, this learning group showed effects of the spatial learning and decreased diffusivity in the left hippocampus and right para-hippocampus after only 2 h of practice. Rats trained on the water maze for only 2 h showed decreased diffusivity in the hippocampi (greater decreases on the left) and increases in markers for synaptic changes, astrocyte changes, and in brain-derived neurotrophic factor (BDNF), which may be a marker for long-term potentiation. Hofstetter et al. showed that in both rats and humans, diffusivity decreased as a result of learning in the fornix connecting the hippocampus to the diencephalon. Moreover, this decrease was correlated with the changes in diffusivity in the hippocampus, although no histological measures in the rats were reported. Tavor et al. repeated this same experiment with both a standard diffusion tensor model and with a more complex diffusion sequence and model (the composite hindered and restricted model of diffusion (CHARMED) proposed by Assaf and Basser (2005)). They again found decreased diffusivity in the left hippocampus, bilateral para-hippocampal gyrus and the bilateral insula, and showed that the changes in the left hippocampus and right parahippocampal gyrus were accompanied by an increase in the volume of water in the restricted compartment of the CHARMED model.

Neuroplasticity resulting from short-term learning has also been explored by comparing fMRI-measured functional connectivity (FC) in within-subject training experiments. Functional connectivity is a measure of the correlation or covariance across time of changes in the levels of activation among spatially separated brain regions. One of the earliest studies using the technique was in fact a learning study (Büchel et al., 1999). Participants learned spatial locations of presented objects, and despite decreases in activation with repeated presentations of the item (repetition suppression), the correlation of the activation time series between ventral object processing cortex and dorsal spatial processing cortex increased with learning. This task-related FC is thought to capture the dynamic functional changes in regional communication across networks of areas involved in the learning task, and it could be a manifestation of a number of relatively low-level short-term neuroplastic processes (e.g., LTP, synaptogenesis, astrocyte signaling). In addition, a number of studies have also used *intrinsic* FC, (sometimes referred to as resting state FC (rsFC) because it is often measured without the participant performing a specific task) to look at the effect of learning (reviewed by Kelly and Castellanos (2014)). Such intrinsic connectivity increases are found in humans for simple motor learning (Albert et al., 2009) and for learning to navigate in a virtual environment (Woolley et al., 2015). There is ample evidence this measure of functional connectivity, involving very slow low-frequency correlations between regions while the participant is unoccupied with an experimenter-imposed task, increases following many types of learning, although whether such changes should be considered functional or structural remains controversial.

Here we investigate how a diffusion-based measure of spatial learning, presumably reflecting structural changes in the brain, is related to changes in brain function. We attempt for the first time to relate the learning-related changes in diffusivity in the spatial encoding network to fMRI-measured changes in both intrinsic FC and task-related FC across the network. The much slower, intrinsic synchronized fluctuations in BOLD signal intensity among regions are thought to reveal the networks of connectivity resulting from a history of co-activation (see Buckner et al. (2013) and Raichle (2011), for recent reviews), whereas task-related FC is thought to reveal online changes in communication among regions necessitated by performance of the cognitive task. We ask whether very recent history (over the course of the previous hour) can effect changes in these networks that can be related to the learning that has occurred during that time. We examine whether a period as short as 45 min of practice in traversing the same virtual route is sufficient to produce the changes seen in the previous studies.

The methodology explores whether the learning changes can be detected with a much shorter diffusion scan that nevertheless provides higher angular resolution. This speed-up benefits from the simultaneous multi-band stimulation (SMS) imaging (Sotiropoulos et al., 2013) used in the Human Connectome Project, but with significant improvements. The design of the experiment is shown in Fig. 1.

Materials and methods

Participants

Twenty-nine right-handed adults (26 females, 3 males, between the ages of 19 and 31 years, *Mean* = 22 years, *SD* = 2.9 years) from the Carnegie Mellon University community participated. All participants gave signed informed consent approved by the Carnegie Mellon Institutional Review Boards. All participants had less than 5 h of "action" video game experience (i.e., games played from the first-person perspective and requiring navigation in a virtual environment) during the two years prior to the experiment. These participants could therefore be considered novices who were not familiar with playing action video games. This inclusion criterion is more stringent than that used by other researchers (Bavelier et al., 2011) for considering a participant as a non-video game player. It did, however, result in a much higher proportion of female volunteers who met the criteria.

The participants were assigned to either the Route-Learning or the Control group with the restriction that the groups be as closely matched as possible on age, gender, and ethnicity. The Route-Learning group consisted of 14 participants (*Mean* age = 22.4 years, *SEM* = 0.91, 11 female and three male, two Asian, one African American, nine Caucasian, one Hispanic). The control group consisted of 14 participants (*Mean* age = 22.1 years, *SEM* = 0.6, 13 female and one male, four Asian, 10 Caucasian). An additional participant was removed from the Control group due to excessive motion (see Analyses below) during one of the scans.

Experimental paradigm

To measure functional and structural changes resulting from practice on the driving task, two separate 30-min scanning sessions were conducted for all participants, with a one-hour interval between them. During the interval between the scanning sessions, participants in the Route-Learning group practiced driving the same route 20 times. During this same time the Control group practiced driving 19 different routes (one route being the same one practiced by the Route-Learning group, and repeated at the beginning and end of the intersession practice session).

Driving simulation

For the virtual driving environment, we adapted code from the open source motorsport simulator *Speed Dreams 2.0* (http://www.speed-dreams.org). This software provides high-quality graphics and very realistic visual and physics simulation of driving. We carefully selected the simulated automobile and the virtual routes driven, and adjusted visual and physics simulation parameters such that the driving task would not be difficult to for our sample of very novice players of

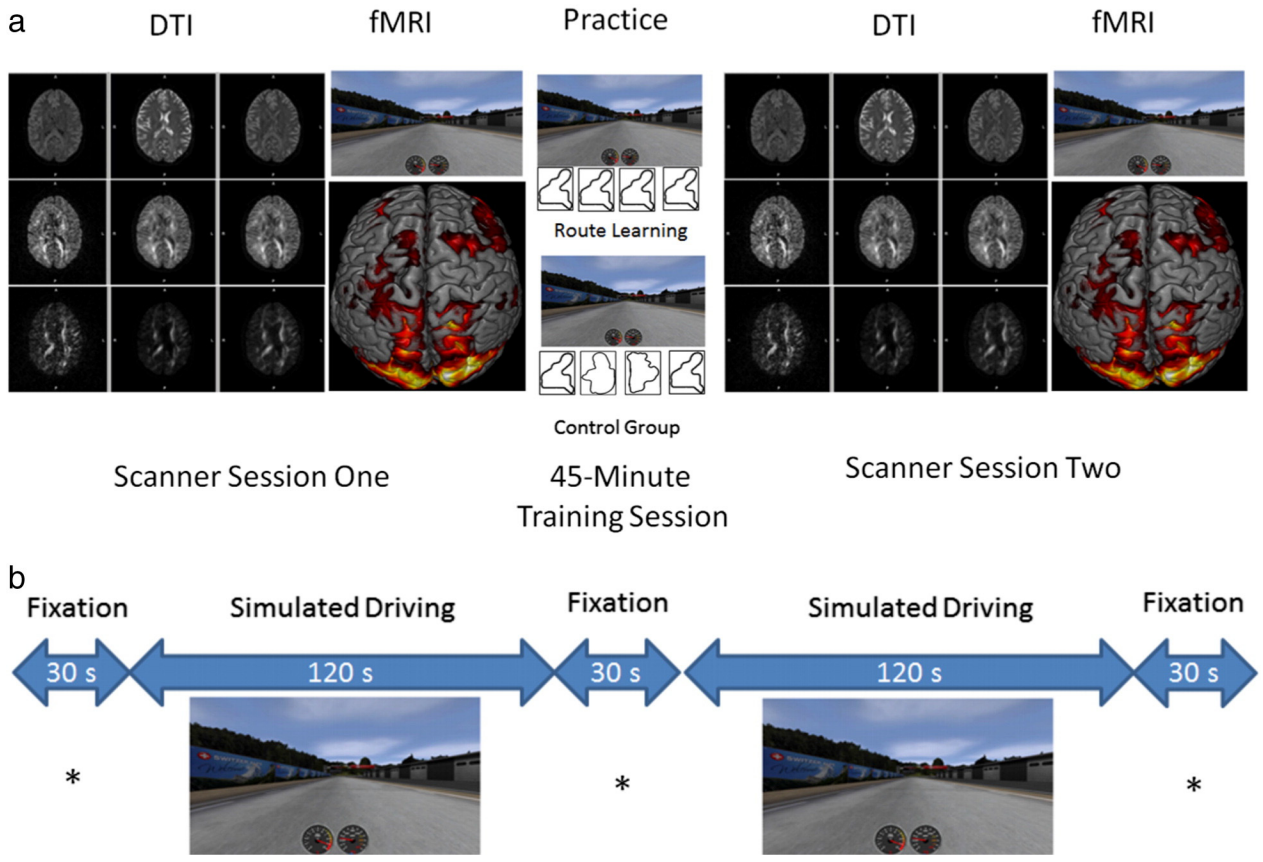

Fig. 1. Design of the experiment. (a) The experiment consisted of two scanning sessions separated by a 1-h interval during which participants in each group practiced the driving task for 45 min. Each scanning session was identical and involved acquisition diffusion images in 30 directions with a b-value of 1000 s/mm^2, and also a functional (T2*-weighted) MRI scan during simulated driving. During the 45-min training session between the scanning sessions, the learning group practiced the driving task by repeating the same route on each learning trial (i.e., lap), for a total of four blocks of five trials each. In contrast, the control group completed the same number of trials but practiced a different spatial route on each trial, with the exception that the route learned by route-learning group was also driven by the control participants at the beginning of the first block and at the beginning of the last block (the figure depicts only the first trial of each block). (b) The fMRI session included two, 2-min simulated drives and three baseline rest periods. Both drives involved the route repeatedly practiced by the route-learning group, and participants were instructed to pretend they were driving the route using a mouse to control the virtual vehicle, in the same way they had been trained in a preliminary practice session.

games requiring navigation through a virtual environment. (A complete specification of all parameter settings and routes chosen are available on request from the corresponding author.) We chose to use a computer mouse as the input device for driving control because it could be used in the scanner environment as well as in the training session. During the training session the simulator ran under a 64-bit version of Windows 8 Pro on an Acer laptop (Aspire V7) with an Intel® Core™ i7 2.4 GHz processor, 8 GB of RAM, and an NVIDA GeForce GT 720M graphics card. The computer mouse was a Logitec wireless M705 optical mouse.

Pre-scanning driving practice

All participants practiced the driving task for approximately 15 to 30 min before any MRI scanning took place. They were first instructed in the use of a computer mouse to control the virtual car, steering it with the mouse and using the left mouse button to accelerate and the right mouse button to brake or reverse the direction of movement. All participants practiced on the same route during this time and this route would not be seen again during the actual experiment. It was intended only to give the groups comparable practice in controlling the car. Participants were told that their goal was to learn to control the car without leaving the road. They were given feedback in the form of "damage" points that accumulated when they left the virtual road, and they were also given feedback about the speed they were driving and their lap time at the end of each drive. Participants were first required to complete the full route without leaving the road. After they met this goal, they were given five more practice trials on the route and told to try to increase their speed. All participants were able to complete the criteria within the 30 min allotted for this phase of the experiment. This practice route was not used again during the experiment, and the pre-training was designed only to give our novice participants sufficient practice on the visuo-motor components of the task to make the lap times and driving accuracy meaningful behavioral measures of learning the more subtle aspects of the task.

MRI sessions

In each MRI scanning session, the paradigm and image acquisitions were identical, both within and across the groups. Participants were told that during the first part of the scanning session structural images of their brain would be taken and that they could relax and watch a movie if they chose to do so. Following scout images used to select slice locations, two diffusion scans were collected using the same 30 gradient vector directions but with opposing phase encoding polarity. Next two gradient echo field mapping sequences were collected, one with each phase encoding polarity, and then a high-resolution T1-weighted anatomical scan was acquired. This structural imaging took approximately 20 min, and was followed by a 4.5 min functional EPI scan. This scan included two, 2-min blocks in which the participant

watched a video of the critical test route being driven by an expert driver. Participants viewed the video through a pair of mirrors over the head coil that reflected the image projected onto a screen anterior to the participants head. They were given a mouse and instructed to pretend that they were controlling the car as they did in the practice. (Note that they did not have actual control the virtual car in the scanner because it was important that the timing and visual stimulation of traversing the virtual route be identical across sessions and across participants. All participants' mouse movements were observed to ensure that they were attending to the task). This functional imaging run also included three, 30-s blocks of rest, during which an "x" was displayed in the center of the screen and the participant was instructed to fixate on it and to relax and clear their mind.

Inter-scan training session

During the intermediate learning session, participants were removed from the scanner and taken to a nearby practice room for training. The Route-Learning group practiced the same route that they had just encountered in the fMRI session of the first scanning session. The learning consisted of four training blocks of five laps of simulated driving of this route, with instructions to try to improve their speed at driving the route while maintaining "safe driving" (i.e., avoiding leaving the virtual road). At the end of each of the four training blocks, participants in the Route-Learning group were asked to complete additional behavioral measures. They were given 8 screen shots of random locations along the route, and asked to arrange these in the order they would be encountered while driving. In addition, they were asked to sketch the outline of the track, and to place letters corresponding to each screen shot at the place on the drawing where they estimated each of the screenshots would be seen. These screen shots were presented in a randomly permuted order for each block and each participant in the Route-Learning group. Participants were given no feedback about accuracy on either the screen shot sorting or the route drawing task.

Participants in the Control group also completed four blocks of driving, but each block consisted of five different routes, with the total distance of all 20 trials being approximately equal to the total distance driven by the Route-Learning group during the inter-scan training session. We also attempted to equate the overall driving difficulty encountered across the two groups by selecting tracks for the control group to practice that on average had comparable numbers of curves and degrees of curvature to the track practiced repeatedly by the learning group. The Control group did not complete the picture sorting or route drawing tasks, and were not expected to learn anything about the routes. They were simply instructed to try to improve their driving speed without sacrificing accuracy of driving, and thus served as an active visuomotor learning control group. Critically, only one route was repeated for this group, once at the beginning (trial 2) and at the end of the training session (trial 19). This was the same route that the Route-Learning group practiced repeatedly and the same route that both groups saw in the scanner during the fMRI imaging sessions.

Image acquisition

All neuroimaging data were acquired on a Siemens Verio (Erlangen, Germany) 3.0 T scanner at the Scientific Imaging and Brain Research Center of Carnegie Mellon University with a 32-channel Siemens receive coil. Both the diffusion-weighted structural images and BOLD-weighted functional images were acquired using the multi-band sequences (version R011 for Syngo VB17A) provided by the University of Minnesota Center for Magnetic Resonance Research (https://www.cmrr.umn.edu/multiband/). Diffusion-weighted, field-mapping, and functional images were all collected as oblique-axial scans aligned with the Anterior Commissure–Posterior Commissure (AC–PC) line at midline.

The diffusion-weighted images were collected with the monopolar cmrr_mbep2d_diff sequence (http://www.cmrr.umn.edu/multiband) in 54 slices (an ascending interleaved acquisition with 2.4-mm-thick slices and no inter-slice gap). The matrix was 96 × 96 and FOV was 230 mm, resulting in 2.4-mm isotropic voxels (TR = 2264 ms, TE = 74.8 ms, multi-band acceleration factor = 3, number of diffusion encoded directions = 30, diffusion b-value = 1000 s/mm^2, number of non-diffusion encoded images = 4, bandwidth = 1860 Hz/Pixel, partial Fourier factor of 6/8). The 30 diffusion encoding vectors were taken from standard Siemens gradient table. Two sets of these images were collected for each participant in each scanning session (pre-training and post-training) with opposite phase encoding directions (anterior > posterior (A > P) and posterior > anterior (P > A)) so that geometric distortions and eddy currents could be corrected using FSL v. 5.0 tools (topup and eddy). The total acquisition time for these two scans was 3 min and 20 s.

Field map images were collected with a vendor-provided Siemens gradient echo sequence (gre_field_mapping) and with the same geometry and orientation as the diffusion data (i.e., 2.4 mm isotropic voxels with 54 slices). These were also collected with both A > P and P > A (TR = 572 ms, TE1 = 5 ms, TE2 = 7.46 ms, flip angle = 70°, bandwidth = 301 Hz/Pixel). Total acquisition time for both of these field maps was 3 min and 40 s.

A T1-weighted MPRAGE volume scan was also collected during each scanning session. This scan used the Siemens turbo-flash sequence with a GRAPPA in-plane phase-encode parallel acceleration factor (i.e., iPat factor) of 2. These data were reconstructed as 176 1-mm sagittal slices with an in-plane resolution of 256 × 256 and a 256-mm FOV, resulting in 1-mm isotropic voxels (TR = 2300 ms, TE = 1.97 ms, TI = 900 ms, flip angle = 9°, bandwidth = 240 Hz/Pixel). Total acquisition time for this scan was 5 min and 21 s.

Finally, each scanning session ended with a functional scan using the Minnesota Multi-band cmrr_mbep2d_bold echo-planar sequence (http://www.cmrr.umn.edu/multiband). An ascending interleaved acquisition was used, with 60 3-mm-thick AC–PC aligned oblique-axial slices and no inter-slice gap. The matrix was 64 × 64 and FOV was 230 mm, resulting in 3-mm isotropic voxels (TR = 1000 ms, TE = 30 ms, bandwidth = 2790 Hz/Pixel, multi-band acceleration factor = 4, and reconstructed on-line with the SENSE1 coil combination method). Each functional run acquired 340 images (5 min and 40 s), once before and once following, the inter-scan training session.

Behavioral analysis

The behavioral data collected during the training included lap times and "damage" scores, for each lap of each route driven. In addition, after each block of four laps, the learning group provided: 1) A score for sorting screen shots taken at equidistant points along the route but with the initial point chosen randomly. 2) A drawing of their estimate of the layout of the route. 3) A score for placement of screen shots at their estimated location on the drawing of the route. The driving data for the two identical routes encountered by both groups (early and late in the training) were analyzed with 2 (time) × 2 (group) mixed ANOVAs. For the Learning group, raw lap time data were fit with a power curve and damage scores were analyzed for a linear trend in the repeated measures. To explore differences in the types of spatial learning tapped by each of the behavioral measures we also conducted simple regression among these behavioral measures and stepwise multiple regression analyses to evaluate their relationships to the neuroimaging data. These analyses were carried out in SAS v. 9.3 software (http://www.sas.com/en_us/software/analytics/stat.html) using Proc Mixed and Proc Reg.

The landmark sorting task was scored by following the general procedure reported by Sagi et al. (2012). For each of the eight screenshots in each test, one point was given for each of the other screenshots that it correctly preceded in the participants sorting response. If the participant placed the first image encountered on the track in the first position, they were awarded 7 points. If they placed the second image encountered in the second position the received 6 points, and so forth.

Thus a perfect arrangement would receive a maximum score of 28 (i.e., 7 + 6 + 5 + 4 + 3 + 2 + 1), and a completely reversed ordering would receive a score of 0. The landmark placement task was scored in the same way and so highly correlated with the sorting measure that it was not analyzed further.

Each route sketch was saved as a digital file of 591 × 724 pixels. For each sketch, a Procrustes analysis (Gower, 1975) was carried out to quantify the dissimilarity between the sketch and the reference template map of the route. This analysis first calculates an optimal superimposition of each sketch to the template by translating, rotating, and scaling the sketch to match the template by minimizing the sum of squared deviation between the two based on only these transformations. Following this Procrustean superimposition, the root mean squared error in the fit provides a "dissimilarity" or "distance" measure of difference between the sketch and the template.

Image analysis

Preprocessing of the diffusion-weighted images (DWI) made use of tools from FSL v. 5.0.8 (http://fsl.fmrib.ox.ac.uk/fsl/fslwiki/) (Smith et al., 2004), and code written in-house for motion correction of diffusion data (Jung, 2010; Jung et al., 2013) running under MATLAB®, v. R2011a (www.mathworks.com/products/matlab). Brain-only masks of images at each stage of the following procedures were extracted using the FSL's "bet2." Estimation and correction of geometric distortion was carried out for each session (pre-training and post-training) using the eight non-diffusion-weighted images (b-value = 0), four collected with each phase encoding direction (A > P, P > A) (Andersson et al., 2003). FSL's "topup" tool was first used to estimate a warp-field and the data were subsequently resliced and the two diffusion runs averaged using the "applytopup" tool. FSL's "eddy" tool was then used to simultaneously model the eddy current effects and head motion effects in the run-averaged data using default values for all parameters (i.e., a quadratic spatial model, no spatial filtering, and five iterations of the non-linear estimation).

Additional pre-processing involved generation of an estimated diffusion-weighted image for each corrected diffusion-weighted image on the basis of average signal intensities across the corrected unweighted (b-value = 0) images (Jung, 2010; Jung et al., 2013). Given the acquisition parameters of each image the estimated signal for each voxel in each diffusion direction can then simply be derived from the Bloch–Torrey equation (Torrey, 1956), resulting in a "simulated" diffusion-weighted image that is perfectly co-registered to the mean of the corrected un-weighted images. We then used each simulated image as the target for a 12-parameter affine co-registration with the corresponding corrected DWI. This estimation and reslicing was carried out with FSL's "mcflirt" program, using a correlation ratio cost function. Finally, each of the affine transformation matrices computed above were combined, and a single reslicing of the original data was carried out with FSL's "applywarp" and the direction of the diffusion vectors were rotated on the basis of this combined transformation prior to fitting a weighted-least squared diffusion tensor model with FSL's "dtifit."

Because the pre-training and post-training scanning involved separate scanning sessions, with the participant repositioned as closely as possible, but not perfectly for the post-session scan, an additional co-registration was required to compare the before and after repeated measures of DTI metrics within each participant. The fractional anisotropy (FA) images calculated for each session provide exquisite contrast for carrying out this co-registration and so these were used in preference to the mean of the un-weighted (*b-value* = 0) images, and because FA is a normalized measure (the standard deviation of three eigenvalues from the DTI fit), changes in signal due to scanner drift between sessions can be ignored. Specifically, a forward (pre- to post-training) and backward (post- to pre-training) 12-parameter affine transformation matrix was calculated with FSL's "flirt" for each participant's two FA images, and the half-way transformation matrix of each was used to re-slice the data into a position half-way between the two FA images. This method ensures that both the pre- and post-training images undergo comparable spatial blurring during the re-slicing process. These transformations were then applied to each of the scalar images resulting from the tensor fit (i.e., λ1, λ2, λ3, FA, MD).

To allow comparison across participants and groups, we used FSL's "fnirt" tool with default parameters for FA to FA non-linear co-registration, to estimate the warping from each participants pre- and post-training FA map to the FMRIB_FA_1mm template included in FSL. This nonlinear warping was applied to each of the scalar DTI measure maps for each participant and session. This procedure is identical to that used in the Tract-based Spatial Statistics (Smith et al., 2006), except that for the diffusivity data we used a voxel-based approach rather than projection of diffusion data to the white matter skeleton defined by peak FA, because our interest is in diffusion changes in not only in white matter but also in gray matter. Following the initial transformation to the FMRIB_FA_1mm template, a study specific template was created by averaging all FA data from both groups and both sessions, and this was used as the target for final non-linear spatial normalization of each FA image. These final warp coefficients were then applied to all of the scalar DTI-measure maps. For the FA data we also generated a study-specific white matter skeleton and applied the traditional TBSS approach of projecting FA values to a mean FA skeleton.

Although FA is a normalized measure, the diffusivities are not, and they are therefore susceptible to any number of equipment- or environment-related changes between the scans. We tested this directly by comparing pre- and post-training non-DWI (*b-value* = 0) means for differences in signal (this was carried as a paired *t*-test across all participants using non-parametric permutation testing with FSL's "randomize" tool with 50,000 permutations and threshold-free cluster enhancement parameters set to the default values for 3D rather than 2D data to correct for multiple comparisons) (Smith and Nichols, 2009). There were no reliable differences between sessions at a corrected $P < .05$ level, but there were differences at an uncorrected $P < .05$, suggesting some unknown systematic change that could affect the diffusivity measures. Global normalization (i.e., adjusting the T2-weighted signal intensity across the brain to have the same mean within a participant between the two sessions) of the non-DWI means removed any trend of differences between scans in an otherwise identical analysis. We therefore included the mean whole-brain T2-weighted signal intensity of the non-DWI images from each session and participant as a covariate in all further analyses of diffusivity changes. These analyses were also performed using FSL's "randomise" utility and involved 50,000 permutations and TFCE correction for multiple comparisons with alpha = .05 corrected.

Pre-processing of the T2*-weighted EPI data was carried out with a combination of tools from MATLAB® v. R2011a, SPM12, and FSL v. 5.0.8. Because the position of the head was not perfectly aligned between sessions, we first corrected each run separately for geometric distortions using the gradient echo field map collected within the same session and FSL's "prelude" and "fugue" tools. Motion was then estimated separately within each run with FSL's "mcflirt" using default (six-parameter affine, reference as the temporally middle image, normalized correlation cost functions settings) (Jenkinson et al., 2002) and the "fsl_motion_outliers" script was used to calculate the temporal derivative of the root-mean-square variance (DVARs) (Power et al., 2012) between each image and the next and motion outliers were identified as any point with a DVAR value greater that the 75th percentile + 1.5 times the interquartile range. Indices for images considered outliers were saved in a regressor so that their effect could be removed (i.e., "scrubbed") in all general linear models (GLMs) to be conducted. There was no difference between groups in the mean DVAR metric and no group × time interaction, although there was a main effect of time, with higher motion in the post-training scan (Pre-training *Mean* = 11.3, *SEM* = 0.4; Post-training *Mean* = 12.0, *SEM* = 0.4; $F(1, 26) = 11.96$, $P < 0.002$). Despite this

small difference, the number of outliers identified in each participant did not show main effects of group or time, nor an interaction (*Mean* = 25.2, *SEM* = 10.0).

To allow comparison across sessions, a co-registration strategy similar to that used for the DWI data was carried out. The mean of each motion corrected fMRI run was used to calculate a forward (pre- to post-training) and backward (post- to pre-training) six-parameter affine transformation matrix with FSL's "flirt" tool. The half-way transformation matrix of each was then saved to later re-slice the data into a position half-way between the two means. These means were averaged for each participant and a non-linear transformation between each participant's mean EPI image and the MNI averaged 152-participant T2-weighted template was carried out using FSL's "fnirt" tool with default registration schedule parameters for intra-modal T2-weighted registration. All participants' data were then averaged to create a study specific EPI template, and the transformation from the participant's mean to this new template was saved as the final non-linear warping. (Note that final re-slicing of the data was all done in a single step that concatenated all the pre-calculated transformation matrices together and used a final sync interpolation to 2-mm isotropic voxels in MNI space.)

For the analysis of intrinsic functional connectivity, each participant's co-registered, motion-corrected, and spatially-normalized data were band pass filtered using FSL's "fslmaths" tool, retaining frequencies between approximately 0.01 Hz (high-pass sigma = 50) and 0.1 Hz (low-pass sigma = 5). A region of interest was defined by the voxels within the left hippocampus showing a reliable decrease in mean diffusivity for the Learning group in the group analysis of the diffusion data, and the time-series of these 126 voxels were averaged within each participant. The averaged time-series of all voxels within each region of interest defined by the automated anatomical labeling (AAL) atlas (Tzourio-Mazoyer et al., 2002) were also calculated for each participant, and all pairwise correlations were calculated among regions of interest, Fisher-z-transformed, and submitted to a group (2) × time (2) × Region (72) mixed ANOVA. Analysis of task-related functional connectivity was identical, except that the data were not temporally filtered, and only voxels with the AAL regions that exceeded a threshold of $t > 3.0$ for the driving minus baseline activation general linear model (GLM) contrast described below, were considered. AAL regions with fewer than eight voxels showing a response to the task at this threshold were ignored. These criteria thus focused the task-based connectivity analysis on regions that were truly involved in the simulated driving task. For both measures of connectivity, the analysis was carried out only on the two 120 s blocks of simulated driving carried out in the scanner, and excluded both the fixation baseline intervals and the first 10 s of simulated driving, to remove the influence of the onset of visual stimulation and motor responses from the correlation of time series across regions.

In addition, changes in intrinsic and extrinsic FC were examined on a voxel-wise basis using the filtered time course in the same seed region in the left hippocampus of each participant for the calculation of partial-correlation maps using FSL's FEAT and including motion parameters and DVAR-based outliers as additional confound variables. The partial-correlation maps for each participant and each timepoint were Fisher-z transformed. Voxel-wise group analyses of the whole-brain correlation maps were then conducted in a voxel-wise mixed ANOVA including group (learning vs. control) and time point (pre vs. post) factors.

Activation in the fMRI data was examined using SPM12. The co-registered, motion-corrected, and spatially normalized data were smoothed with a eight-mm full-width at half-maximum Gaussian spatial filter and submitted to a first-level GLM for each participant. Regressors for the pre-training simulated driving intervals, and the post-training simulated driving intervals were convolved with the default SPM12 hemodynamic response function, and an additional covariate specifying motion outliers was included as a finite impulse response function, as well as a high-pass filter (with a period of 120 s) to remove linear trends in the data. The first-level models were fit with an autoregressive (AR(1)) error covariance structure using restricted maximum likelihood estimation (REML). The contrast of beta values between simulated driving and rest was calculated, as well as the difference in beta values between the pre-training and post-training sessions. These contrasts were entered into a second-level group (2) × time (2) voxel-wise analysis using a family-wise cluster-size correction for multiple comparisons based on random field theory (with an initial cluster-forming criterion of $P < .0001$).

Results

Diffusion-weighted changes with learning

The principal prediction was that a mean diffusivity (MD) decrease in the hippocampus (reflecting microstructural changes in the regions) would be accompanied by an increase in functional connectivity (reflecting changes in brain function) between hippocampus and other cortical regions involved in learning. Moreover, both types of changes were expected to be related to the degree of performance improvement on the route-learning task. As an indication of the specificity of the effect, such route-learning-related hippocampal changes were not predicted for a control group that had a similar amount of practice in the driving task, but not on any single route. Below each of the component results are described first, followed by a description of the structural–functional concurrence.

The structural prediction was confirmed by reliably decreased MD in the left hippocampus of the route-learning group (peak $t(13) = 2.48$, $P < .02$). Although the effect was left-lateralized, as shown in Fig. 2a, overall diffusivity in both the left and right hippocampi decreased reliably for the participants who repeatedly practiced the same route. In contrast, participants who had comparable amounts of driving practice but on a number of different routes showed no change in diffusivity in either the left hippocampus or the right hippocampus (Fig. 2b).

The region of the left hippocampus showing the reliable decrease in the voxel-wise analysis constitutes only a fraction of the total volume of the structure (approximately 14%). The center of mass of the region was at −28, −29, −7, and the peak decrease was at −34, −28, −10, in MNI coordinates. This location is somewhat more lateral, posterior, and superior to the previously reported location of the peak voxels showing MD decrease in a similar route leaning task (Sagi et al., 2009). Nevertheless, the left hippocampal cluster shown in Fig. 2a extended from −42 to −4 mm in the anterior–posterior dimension adding confidence to the finding of a left hippocampal MD decreases with route learning. Comparison of the cluster with the Jülich histological atlas (Amunts et al., 2005; Eickhoff et al., 2007) indicated that this region included portions of the dentate gyrus and the cornu ammonis. In addition, its relatively posterior location is consistent with the hippocampal area found to increase in volume with experience in driving a London taxi cab (Maguire et al., 2000).

Several other (left-lateralized) white and gray matter regions also showed mean diffusivity decreases in the spatial learning group, as assessed with a voxel-wise mixed ANOVA (Fig. 2c). Although not predicted, neuroplasticity in some of these cortical regions seems plausibly related to the learning task. For example, the precuneus has been associated with egocentric navigation in a number of imaging studies (Schindler and Bartels, 2013; Chadwick et al., 2015). The role that other regions might play is less clear, though, and we therefore analyze below the functional connectivity among these areas showing learning-related structural change. The control group showed no changes in MD in the hippocampus or parahippocampal gyrus. Both groups, however, showed reduced diffusivity in the left corona radiata ($P < .05$ corrected) although the changes were in the left external capsule for the control group and in the extreme capsule for the route-learning group (see Supplementary Fig. 1). If changes in less complex visuo-motor learning can be detected with this method, similar decreases in MD in the two groups would also be expected in other areas.

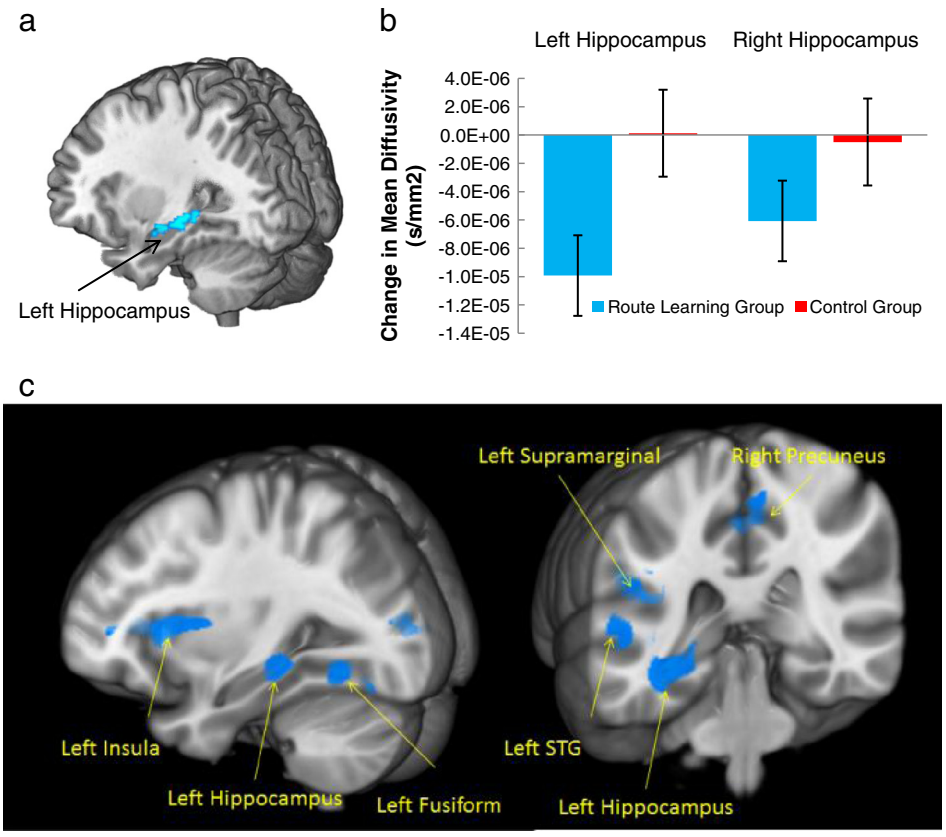

Fig. 2. Decreased mean diffusivity (MD) in the left hippocampus as a result of spatial-route learning. (a) Area of the left hippocampus showing a reliable decrease in MD between the pre-training diffusion-weighted image acquisition and the post-training acquisition for the route-learning group but not the control group ($P < .05$, corrected for all voxels within the brain using Threshold-Free Cluster Enhancement). (b) Change in diffusivity between the scans in the hippocampus of each hemisphere for the two groups. These data average all voxels in regions of interest for the entire left hippocampus and right hippocampus. In contrast to the control group, the route-learning group shows reliable decreases for both of these measures. Error bars represent the standard error of the mean. (c) Additional regions of decreased diffusivity following training in the spatial route-learning group. Other cortical areas showing diffusivity-sensitive neuroplastic changes included the precuneus (6, −64, 30) the left superior frontal gyrus (−18, 2, 52), the left insula (−32, 16, 6), the left supramarginal gyrus (−50, −36, 24), the left superior temporal gyrus (−60, −20, 2), and the left fusiform gyrus (−30, −60, −12). All coordinates are in MNI space.

fMRI-measured intrinsic functional connectivity

It is important to determine whether the diffusivity changes with route-learning described above are related to changes in brain function, specifically, to changes in intrinsic functional connectivity. The band-pass filtering of the time-series data, retaining only frequencies between 0.01 and 0.1 Hz, should effectively remove any correlation in the data associated with the rapid activation changes involved in the simulated driving task, as well as with artifacts from heart rate, and respiration (Lowe et al., 1998). This analysis was restricted to connections involving the portion of the left hippocampus showing a reliable decrease in the MD data for the learning group. The intrinsic connectivity was calculated between the mean time course of this region and that of each of 73 cortical and subcortical regions of interest (defined by the Anatomical Automatic Labeling (AAL) atlas (Tzourio-Mazoyer et al., 2002)). A mixed ANOVA (group × time × connection) on these data showed no evidence of three-way interaction, although there was of course a robust main effect of connection ($F(70, 1820) = 21.85$, $P < .00001$)). Of most interest, however, was an overall group by time interaction ($F(1, 26) = 7.00$, $P < .02$). The learning group clearly showed a larger increase in these low frequency physiological fluctuations of bold signal between the left hippocampus and the rest of cortex (see Fig. 3a). A relationship between changes in these low frequency fluctuations and changes in MD may reflect relatively long-lasting changes in communication among these regions by virtue of repeated co-activation during the training period. The finding supports the contention that the diffusivity changes are not simply epiphenomena, resulting from activity within the hippocampus, but rather, they represent functionally relevant structural changes.

Although knowledge of the anatomical connectivity linking the affected region of the left hippocampus to the rest of the brain in humans is sparse, there are a number of regions we expected to co-activate with the hippocampus during spatial learning and hence show functional or structural plasticity as a result of the learning. These regions include the bilateral temporal regions involved in visual motion processing, and the left and right intraparietal sulci involved in spatial processing. In addition, given manual motor requirements, one might expect that spatial procedural learning could involve changes in functional or structural connectivity with the contralateral motor hand area in the left precentral gyrus, with the left supplementary motor area, and with the ipsilateral cerebellum. We therefore conducted separate ANOVAs for the fMRI-measured intrinsic connectivity between each of these regions and the left hippocampal region of route-learning decrease in MD.

The route-learning group showed reliably greater increases in intrinsic functional connectivity between the left hippocampal region of interest and the right posterior inferior temporal gyrus (interaction $F(1, 26) = 7.27$, $P < .05$, corrected) right anterior inferior temporal gyrus (interaction $F(1, 26) = 7.05$, $P < .05$, corrected), the right intraparietal sulcus (interaction $F(1, 26) = 4.54$, $P < .05$). No Group by Time interaction was found for any of the left hemisphere homologues of these regions (all $Fs < 1$).

In contrast to the strongly right-lateralized changes in intrinsic connectivity for regions involved in the visuo-spatial learning aspects of the driving task, the changes in regions typically involved in procedural aspects of motor learning were left-lateralized (all of the participants were right-handed). In such regions (precentral gyrus, supplementary motor area), reliable interactions were found only in the *left hemisphere*

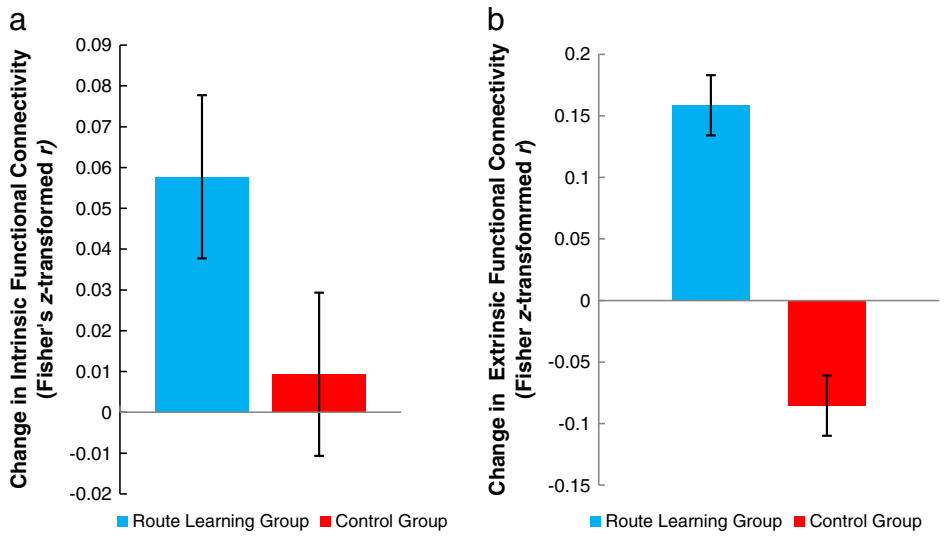

Fig. 3. Functional connectivity changes with route learning. (a) Increase in intrinsic functional connectivity (low frequency fluctuations among anatomical regions) for each group between the left hippocampal area showing diffusivity changes in the route-learning group and all other regions. (b) Increase in task-related functional connectivity for each group before and after training, averaged across activated voxels among pairs of 73 cerebral regions (only time-series for voxels with a t-value > 3.0 for the contrast of simulated driving with fixation were included). Following the training, only the route-learning group showed a reliable increase in functional connectivity related to the driving task performed in the scanner. Error bars represent the standard error of the mean.

(for the precentral gyrus (interaction $F(1, 26) = 5.54$, $P < .05$); for the left supplementary motor area (interaction $F(1, 26) = 5.02$, $P < .05$). In the right hemisphere homologues, neither of the interactions approached significance (both Fs < 1.0). All three regions of interest in the cerebellum, however, showed the reliable group × time interaction. (For the vermis, interaction $F(1, 26) = 6.54$; for the left cerebellum, interaction $F(1, 26) = 5.38$; and for the right cerebellum, interaction $F(1, 26) = 4.78$, $P < .05$).

We also performed an exploratory analysis of the intrinsic connectivity among the regions shown in Fig. 2. Although there were no reliable group by time interactions when the analysis was restricted to these regions localized independently by the diffusivity changes in the learning group, there was a reliable main effect of group for the functional connectivity between the precuneus and the left insula and ($F(1, 52) = 4.55$, $P < .05$), with the learning group showing higher intrinsic connectivity than controls. There was also a trend toward an increase in connectivity across groups for the pair involving the precuneus and the left hippocampus ($F(1, 52)$, $P < .10$). As noted above, it is not surprising that both the structural and functional connectivity of the precuneus might be affected in the present task.

Finally, when the same data were analyzed using the voxel-wise, seed-based approach, no reliable differences between groups or between scans were found after correction for multiple comparisons. There was, of course, highly reliable intrinsic functional connectivity between the hippocampal seed and a variety of cortical and subcortical structures within each scanning session. Supplementary Fig. 2 displays the simple main effect of intrinsic connectivity with the left hippocampal seed region for each of the groups and each of the time points.

fMRI-measured task-based functional connectivity

It was expected that there would be an increase in task-related functional connectivity with route learning, as has been previously reported in other learning tasks (Büchel et al., 1999; Schipul et al., 2012). Unlike the intrinsic connectivity analysis, this analysis applies no temporal filtering, allowing dynamic changes in the functional co-activation of regions resulting from the driving task to be detected. The task-related functional connectivity of the two groups was very similar prior to training, but the route-learning group had significantly higher functional connectivity following the training session, as summarized in Fig. 3b. A group by time mixed-model ANOVA with connection treated as a random variable, showed a reliable interaction between group and time in overall functional connectivity ($F(1, 26) = 246.76$; $P < .0001$).

The group difference in the change in task-based functional connectivity was not specific to connections involving the left hippocampal MD-defined region. A group × time × connection mixed ANOVA that was restricted to connections with the left hippocampal MD-defined region showed no reliable three-way interaction, nor a group × time interaction (Ps > .80). Furthermore, separate planned group × time mixed ANOVAs were conducted based on the same predictions as those for intrinsic connectivity between the left hippocampal region and bilateral temporal, intraparietal, precentral, supplementary motor, and cerebellar regions. None of these connections (which had shown a group × time interaction for intrinsic connectivity) showed this interaction for the task-related functional connectivity data. Thus, the overall task-relevant activity became more synchronized in the route-learning group, indicating an improvement in brain function with training, but these changes were not specific to connections between the left hippocampus and other regions.

Relation between structural changes and behavioral performance changes

The prediction that decreases in diffusivity would be related to increases in performance on the task, was also supported by the data. Differences in lap times between each participant's first and last drive were calculated for the route that was common between the two groups. (The control participants drove this same track in only the first and last block of the training session, as described in the Materials and methods section.) At the conclusion of training, the route-learning group was significantly faster ($t(26) = 2.39$, $P < .05$; *Mean* = 111 s, *SEM* = 4.0 s) than the visuo-motor learning control group (*Mean* = 125 s, *SEM* = 4.5) on this track, confirming that the route-learning group had learned something beyond motor control of the virtual car during the training (see Supplementary Fig. 3a). Of particular interest is the relationship between the change in diffusivity and change (decrease) in the driving time across participants. The changes in hippocampal diffusivity were reliably correlated with changes in driving performance for the route-learning group ($r = .55$, $P < .05$). There was no such correlation for the visuo-motor-learning control group.

Neither of the other measures of learning (decreased damage, screenshot sorting, route sketching) collected for this group were reliably related to the change in diffusivity.

fMRI activation

The fMRI assessment of BOLD signal during the simulated driving task showed activation in a network of driving-related regions, as displayed in Supplementary Fig. 4. These activation levels were similarly affected by the training in the two groups. A mixed voxel-wise (2) group × (2) time ANOVA found no reliable differences between the two groups in the BOLD activation, at either time point, nor did it indicate any changes in the signal with time either as a main effect or a simple effect within each group.

Additional behavioral changes with learning

As briefly reported above, lap times reliably decreased only in the route learning group ($P < .001$), and this group was reliably faster than the control group in navigating the same route by the end of practice ($P < .001$). The changes in lap times over the course of learning followed a power curve, which explained 65% of the variance (Supplementary Fig. 3a). In addition, the measure of damage (occurring during the car's contact with another object) decreased during the course of learning, but this effect was not significant.

Participants in the route-learning group also improved their ability to correctly order of sequence of landmarks encountered along the driving course. There was a significant linear increase in picture sorting accuracy across the training period ($P < .05$, Supplementary Fig. 3b). Furthermore, the ability to draw the layout of the track they were practicing improved over the course of training, as shown in an example participant's data in Supplementary Fig. 3c and by the significant decrease ($P < .05$) in the mean Procrustes distance between each successive drawing and the template image of the actual course driven (Supplementary Fig. 3d).

The various behavioral measures of learning that showed significant improvement over the course of training were not correlated with each other. A stepwise multiple regression including all of these measures (improvement in lap time, maximum speed, damage scores, screen shot sorting scores, and Procrustes distance between sketches and the true route traveled) was conducted to determine if the separable types of learning independently predicted changes in either diffusivity or functional connectivity. The improvement in lap time together with the improvement in screen shot sorting accounted for 54% of the variance in the decrease in left hippocampal diffusivity ($F(2, 11) = 6.45$, $P < .02$), with the partial correlations for each of these variables explaining significant portions of the variance (for the change in lap times, partial $R^2 = .30$, $P < .05$, and for the change in sorting scores, partial $R^2 = .24$, $P < .05$). Similar analyses for the other regions showing a decrease in diffusivity found no reliable relationships with any of the learning measures, although the relationships were in the expected direction. Changes in sketch dissimilarity explained 18% of the variance in parahippocampal diffusivity change ($P = .13$), and sorting scores explained 19% of the change in intrinsic functional connectivity ($P = .12$) between the left hippocampus and the rest of the cortex, but no other effects approached significance.

Individual difference measures of spatial ability were equivalent between the two groups. One highly-relevant measure of individual differences in cognitive ability, the Santa Barbara Sense of Direction Scale (Hegarty et al., 2002), predicted the route-learning participants' increase in speed on driving the course. This prediction held both early in the training session (for the first block the correlation between the SBSOD and the increase in speed was .57 ($P = 0.05$)) and late in the training session (for the fourth block this correlation was .53 ($P = 0.06$)). No similar relationship was found for the control group, and no similar relationship was found with mental rotation ability measured by the Vandenberg and Kuse (1978) test, which assesses the ability to mentally visualize and perform imagined transformations on objects in the environment. The results indicate that only the ability to update one's position in space influenced the ability to learn the route with repeated practice.

Discussion

The new findings reveal how structural changes in the hippocampus are associated with spatial learning (as assessed with mean diffusivity) and are related to BOLD signal changes in other cortical and subcortical regions. The major new result is that increases in intrinsic connectivity, resulting from the route learning and structurally plastic in nature, occur between areas of gray matter involved in spatial navigation and the portion of the left hippocampus that shows the decrease in mean diffusivity. This finding establishes the critical link between a structural brain change and a functional brain change during learning.

The findings also show that mean diffusivity changes in the left hippocampus and parahippocampal gyrus are detectable after only 45 min of training on an implicit route-learning task. These changes may provide an important marker for gray matter structural change resulting not only from route learning, but also learning and memory related to neuroplasticity in general. The findings also show that we may not yet have reached the lower limit on how much training is necessary to produce such changes, indicating remarkably rapid short-term structural neuroplasticity of the hippocampus. The study provides an important, independent confirmation of the meticulous previous work carried out in a single laboratory (Blumenfeld-Katzir et al., 2011; Sagi et al., 2012; Hofstetter et al., 2013; Tavor et al., 2013). Like the previous work, this study shows that the magnitude of diffusivity changes in hippocampus are significantly related to the behaviorally-measured magnitude of the learning changes.

Task-related functional connectivity involving the synchronization of BOLD activation among gray matter regions was also sensitive to the learning effect, as indicated by an overall increase in this measure of information processing capacity and interregional communication in the group that was trained on the single route. These learning-related changes in task-induced functional connectivity were not specific to areas showing diffusion-weighted changes. We suggest that they may reflect more cognitive or strategic changes resulting in greater cortico-cortical co-activation of distant task-relevant regions. In contrast, learning-related changes in intrinsic connectivity were found for connections with the hippocampal region of gray matter structural change. Thus, the implicit learning of spatial or navigational information appears to indeed be reflected in structural neuroplasticity, rather than in more dynamic or cognitive changes in information processing for navigation (e.g., a conscious change in strategy).

It is now clear that intrinsic (or resting-state) functional connectivity found in the synchronous time-courses of BOLD signal among regions is the result of spontaneous and low-frequency volleys of neuronal activity, as demonstrated by simultaneous measurements of fMRI data and local field potentials, infra-slow fluctuations, delta-band activity, direct current potentials and other electrophysiological indices provided by EEG and ECoG. In addition, fluctuations in measures of regional oxygen availability, cerebral blood flow, and vasomotion appear important in coupling the neuronal and BOLD responses (Lu and Stein, 2014). The large proliferation of studies measuring it is a testament to the widespread acceptance of its importance in understanding the brain. In terms of metabolic cost, its maintenance likely dwarfs that required by task-related activity (He and Raichle, 2009). Despite such insights into its mechanisms, its evolutionarily beneficial effect on survival remains elusive. It reflects anatomical connectivity but is not constrained by it (Raichle, 2011).

We suggest that the increase in intrinsic connectivity seen in the route-learning group is the result of co-activation of the extraordinarily neuroplastic hippocampal place encoding regions and the network of spatial processing areas that receive input and output. Although this synchronization of low frequency BOLD signal fluctuations is referred to as *intrinsic* in the literature, it nevertheless changed in the short term as a function of training, so it is not intrinsic in the sense of being inherent or hard-wired into the system.

The specificity of the changes in learning-related functional connectivity was remarkable. Connectivity increased between the posterior dorsal region of the human dentate gyrus (a region known to be involved in spatial learning) (Moser and Moser, 1998; Brown et al., 2014), and the right intra-parietal sulcus, right anterior and posterior temporal areas (cortical regions activated strongly in navigation and spatial memory tasks). These findings are consistent with both the anatomical connectivity among these regions (Schmahmann and Pandya, 2006), and with the functional activation of these particular cortical areas in navigation and spatial memory tasks (Gomez et al., 2014).

Conclusions

Diffusion changes were shown to provide an alternative marker of spatial route-learning that may be more sensitive to short-term spatial learning than activation or task-evoked functional connectivity changes. Mean diffusivity changes in the left hippocampus occurred only in the learning group. The magnitude of the diffusivity changes are related to behavioral improvement on the task, and the regions that are connected to the human posterior-dorsal dentate gyrus of the left hippocampus also show short-term changes in slow (<0.1 Hz), but synchronized, fluctuations in the fMRI-measured BOLD signal. The findings suggest that short-term quantitative changes in intrinsic connectivity may in fact be more easily detected than microstructural changes in white matter, and can clearly be related to microstructural changes in the hippocampus. The combination of the two methods may provide a narrow enough spatial and temporal window to employ in microgenetic (Siegler, 2006) longitudinal studies of many types of learning, and promises to extend our understanding of learning in humans to more fine-grained levels of analysis.

Acknowledgments

This research was supported by the Office of Naval Research (grant number N00014-13-1-0250). We thank Xiaolu Lei for software development and collection of the data, and Theodore DePietro and Nicholas Diana for additional programming help. We also thank Andrew Bauer, Vladimir Cherkassky, Robert Mason, and Ying Yang for many helpful comments on the paper.

Appendix A. Supplementary data

Supplementary data to this article can be found online at http://dx.doi.org/10.1016/j.neuroimage.2015.10.015.

References

Albert, N.B., Robertson, E.M., Miall, R.C., 2009. The resting human brain and motor learning. Curr. Biol. 19, 1023–1027.
Amunts, K., Kedo, O., Kindler, M., Pieperhoff, P., Mohlberg, H., Shah, N.J., Habel, U., Schneider, F., Zilles, K., 2005. Cytoarchitectonic mapping of the human amygdala, hippocampal region and entorhinal cortex: intersubject variability and probability maps. Anatomy and Embryology, pp. 343–352.
Andersson, J.L.R., Skare, S., Ashburner, J., 2003. How to correct susceptibility distortions in spin-echo echo-planar images: application to diffusion tensor imaging. NeuroImage 20, 870–888.
Assaf, Y., Basser, P.J., 2005. Composite hindered and restricted model of diffusion (CHARMED) MR imaging of the human brain. NeuroImage 27, 48–58.
Bavelier, D., Green, C.S., Han, D.H., Renshaw, P.F., Merzenich, M.M., Gentile, D.A., 2011. Brains on video games. Nat. Rev. Neurosci. 12, 763–768.
Blumenfeld-Katzir, T., Pasternak, O., Dagan, M., Assaf, Y., 2011. Diffusion MRI of structural brain plasticity induced by a learning and memory task. PLoS One 6.
Brown, T.I., Hasselmo, M.E., Stern, C.E., 2014. A high-resolution study of hippocampal and medial temporal lobe correlates of spatial context and prospective overlapping route memory. Hippocampus 24, 819–839.
Büchel, C., Coull, J.T., Friston, K.J., 1999. The predictive value of changes in effective connectivity for human learning. Science 283, 1538–1541.
Buckner, R.L., Krienen, F.M., Yeo, B.T.T., 2013. Opportunities and limitations of intrinsic functional connectivity MRI. Nat. Neurosci. 16, 832–837.
Chadwick, M.J., Jolly, A.E.J., Amos, D.P., Hassabis, D., Spiers, H.J., 2015. A goal direction signal in the human entorhinal/subicular region. Curr. Biol. 25, 87–92.
Colcombe, S.J., Erickson, K.I., Scalf, P.E., Kim, J.S., Prakash, R., McAuley, E., Elavsky, S., Marquez, D.X., Hu, L., Kramer, A.F., 2006. Aerobic exercise training increases brain volume in aging humans. J. Gerontol. A Biol. Sci. Med. Sci. 61, 1166–1170.
Diamond, M.C., Krech, D., Rosenzweig, M.R., 1964. The effects of an enriched environment on the histology of the rat cerebral cortex. J. Comp. Neurol. 123, 111–120.
Draganski, B., Gaser, C., Busch, V., Schuierer, G., Bogdahn, U., May, A., 2004. Neuroplasticity: changes in grey matter induced by training. Nature 427, 311–312.
Draganski, B., Gaser, C., Kempermann, G., Kuhn, H.G., Winkler, J., Büchel, C., May, A., 2006. Temporal and spatial dynamics of brain structure changes during extensive learning. J. Neurosci. 26, 6314–6317.
Eickhoff, S.B., Paus, T., Caspers, S., Grosbras, M.H., Evans, A.C., Zilles, K., Amunts, K., 2007. Assignment of functional activations to probabilistic cytoarchitectonic areas revisited. NeuroImage 36, 511–521.
Engvig, A., Fjell, A.M., Westlye, L.T., Moberget, T., Sundseth, O., Larsen, V.A., Walhovd, K.B., 2011. Memory training impacts short-term changes in aging white matter: a Longitudinal Diffusion Tensor Imaging Study. Hum. Brain Mapp. 33, 2390–2406.
Erickson, K.I., Voss, M.W., Prakash, R.S., Basak, C., Szabo, A., Chaddock, L., Kim, J.S., Heo, S., Alves, H., White, S.M., Wojcicki, T.R., Mailey, E., Vieira, V.J., Martin, S.A., Pence, B.D., Woods, J.A., McAuley, E., Kramer, A.F., 2011. Exercise training increases size of hippocampus and improves memory. Proc. Natl. Acad. Sci. U. S. A. 108, 3017–3022.
Fu, M., Zuo, Y., 2011. Experience-dependent structural plasticity in the cortex. Trends Neurosci. 34, 177–187.
Gomez, A., Cerles, M., Rousset, S., Rémy, C., Baciu, M., 2014. Differential hippocampal and retrosplenial involvement in egocentric-updating, rotation, and allocentric processing during online spatial encoding: an fMRI study. Front. Hum. Neurosci. 8, 150.
Gower, J.C., 1975. Generalized procrustes analysis. Psychometrika 40, 33–51.
He, B.J., Raichle, M.E., 2009. The fMRI signal, slow cortical potential and consciousness. Trends Cogn. Sci. 13, 302–309.
Hegarty, M., Richardson, A.E., Montello, D.R., Lovelace, K., Subbiah, I., 2002. Development of a self-report measure of environmental spatial ability. Intelligence 30, 425–447.
Hofstetter, S., Tavor, I., Tzur Moryosef, S., Assaf, Y., 2013. Short-term learning induces white matter plasticity in the fornix. J. Neurosci. 33, 12844–12850.
Jenkinson, M., Bannister, P., Brady, M., Smith, S.M., 2002. Improved optimisation for the robust and accurate linear registration and motion correction of brain images. NeuroImage 17, 825–841.
Jung, K.J., 2010. Sensitivity of motion estimation to the anisotropic diffusion of white matter in diffusion MRI. Proceedings of the 18th Annual Meeting of the ISMRM. Stockholm, Sweden, p. 4036.
Jung, K.-J., Kohli, N., Yeh, F.-C., Keller, T.A., Zhao, T., 2013. Motion correction in diffusion spectrum imaging using simulated diffusion images at multiple b bands. Proceedings of the 21st Annual Meeting of the ISMRM. Salt Lake City, Utah, USA, p. 3192.
Keller, T.A., Just, M.A., 2009. Altering cortical connectivity: remediation-induced changes in the white matter of poor readers. Neuron 64, 624–631.
Kelly, C., Castellanos, F.X., 2014. Strengthening connections: functional connectivity and brain plasticity. Neuropsychol. Rev. 24, 63–76.
Lövdén, M., Bodammer, N.C., Kühn, S., Kaufmann, J., Schütze, H., Tempelmann, C., Heinze, H.J., Düzel, E., Schmiedek, F., Lindenberger, U., 2010. Experience-dependent plasticity of white-matter microstructure extends into old age. Neuropsychologia 48, 3878–3883.
Lövdén, M., Wenger, E., Mårtensson, J., Lindenberger, U., Bäckman, L., 2013. Structural brain plasticity in adult learning and development. Neurosci. Biobehav. Rev. 37, 2296–2310.
Lowe, M.J., Mock, B.J., Sorenson, J.A., 1998. Functional connectivity in single and multislice echoplanar imaging using resting-state fluctuations. NeuroImage 7, 119–132.
Lu, H., Stein, E.A., 2014. Resting state functional connectivity: its physiological basis and application in neuropharmacology. Neuropharmacology 84, 79–89.
Maguire, E.A., Gadian, D.G., Johnsrude, I.S., Good, C.D., Ashburner, J., Frackowiak, R.S., Frith, C.D., 2000. Navigation-related structural change in the hippocampi of taxi drivers. Proc. Natl. Acad. Sci. U. S. A. 97, 4398–4403.
Maguire, E.A., Woollett, K., Spiers, H.J., 2006. London taxi drivers and bus drivers: a structural MRI and neuropsychological analysis. Hippocampus 16, 1091–1101.
Moser, M.B., Moser, E.I., 1998. Functional differentiation in the hippocampus. Hippocampus 8, 608–619.
Power, J.D., Barnes, K.A., Snyder, A.Z., Schlaggar, B.L., Petersen, S.E., 2012. Spurious but systematic correlations in functional connectivity MRI networks arise from subject motion. NeuroImage 59, 2142–2154.
Raichle, M.E., 2011. The restless brain. Brain Connect. 1, 3–12.
Sagi, Y., Tavor, I., Sasson, E., Pasternak, O., Assaf, Y., 2009. Learning induced structural plasticity in humans using diffusion MRI. NeuroImage 47, S39–S41.
Sagi, Y., Tavor, I., Hofstetter, S., Tzur-Moryosef, S., Blumenfeld-Katzir, T., Assaf, Y., 2012. Learning in the fast lane: new insights into neuroplasticity. Neuron 73, 1195–1203.
Schindler, A., Bartels, A., 2013. Parietal cortex codes for egocentric space beyond the field of view. Curr. Biol. 23, 177–182.
Schipul, S.E., Williams, D.L., Keller, T.A., Minshew, N.J., Just, M.A., 2012. Distinctive neural processes during learning in autism. Cereb. Cortex 22, 937–950.
Schmahmann, J.D., Pandya, D.N., 2006. Fiber Pathways of the Brain. University Press, New York Oxford.
Scholz, J., Klein, M.C., Behrens, T.E.J., Johansen-Berg, H., 2009. Training induces changes in white-matter architecture. Nat. Neurosci. 12, 1370–1371.
Siegler, R.S., 2006. Microgenetic analyses of learning. Handbook of Child Psychology, Cognition, Perception, and Language, pp. 464–510.
Smith, S.M., Nichols, T.E., 2009. Threshold-free cluster enhancement: addressing problems of smoothing, threshold dependence and localisation in cluster inference. NeuroImage 44, 83–98.
Smith, S.M., Jenkinson, M., Woolrich, M.W., Beckmann, C.F., Behrens, T.E.J., Johansen-Berg, H., Bannister, P.R., De Luca, M., Drobnjak, I., Flitney, D.E., Niazy, R.K., Saunders, J.,

Vickers, J., Zhang, Y., De Stefano, N., Brady, J.M., Matthews, P.M., 2004. Advances in functional and structural MR image analysis and implementation as FSL. NeuroImage 23, 208–219.
Smith, S.M., Jenkinson, M., Johansen-Berg, H., Rueckert, D., Nichols, T.E., Mackay, C.E., Watkins, K.E., Ciccarelli, O., Cader, M.Z., Matthews, P.M., Behrens, T.E.J., 2006. Tract-based spatial statistics: voxelwise analysis of multi-subject diffusion data. NeuroImage 31, 1487–1505.
Sotiropoulos, S.N., Jbabdi, S., Xu, J., Andersson, J.L., Moeller, S., Auerbach, E.J., Glasser, M.F., Hernandez, M., Sapiro, G., Jenkinson, M., Feinberg, D.A., Yacoub, E., Lenglet, C., Van Essen, D.C., Ugurbil, K., Behrens, T.E.J., 2013. Advances in diffusion MRI acquisition and processing in the Human Connectome Project. NeuroImage 80, 125–143.
Tang, Y.-Y., Lu, Q., Geng, X., Stein, E.A., Yang, Y., Posner, M.I., 2010. Short-term meditation induces white matter changes in the anterior cingulate. Proc. Natl. Acad. Sci. U. S. A. 107, 15649–15652.
Taubert, M., Draganski, B., Anwander, A., Müller, K., Horstmann, A., Villringer, A., Ragert, P., 2010. Dynamic properties of human brain structure: learning-related changes in cortical areas and associated fiber connections. J. Neurosci. 30, 11670–11677.
Tavor, I., Hofstetter, S., Assaf, Y., 2013. Micro-structural assessment of short term plasticity dynamics. NeuroImage 81, 1–7.
Torrey, H.C., 1956. Bloch equations with diffusion terms. Phys. Rev. 104, 563–565.
Tzourio-Mazoyer, N., Landeau, B., Papathanassiou, D., Crivello, F., Etard, O., Delcroix, N., Mazoyer, B., Joliot, M., 2002. Automated anatomical labeling of activations in SPM using a macroscopic anatomical parcellation of the MNI MRI single-subject brain. NeuroImage 15, 273–289.
Vandenberg, S.G., Kuse, A.R., 1978. Mental rotations, a group test of three-dimensional spatial visualization. Percept. Mot. Skills 47, 599–604.
Woollett, K., Maguire, E.A., 2011. Acquiring "the knowledge" of London's layout drives structural brain changes. Curr. Biol. 21, 2109–2114.
Woolley, D.G., Mantini, D., Coxon, J.P., D'Hooge, R., Swinnen, S.P., Wenderoth, N., 2015. Virtual water maze learning in human increases functional connectivity between posterior hippocampus and dorsal caudate. Hum. Brain Mapp. 36, 1265–1277.
Zatorre, R.J., Fields, R.D., Johansen-Berg, H., 2012. Plasticity in gray and white: neuroimaging changes in brain structure during learning. Nat. Neurosci. 15, 528–536.
Zhang, K., Sejnowski, T.J., 2000. A universal scaling law between gray matter and white matter of cerebral cortex. Proc. Natl. Acad. Sci. U. S. A. 97, 5621–5626.

a b

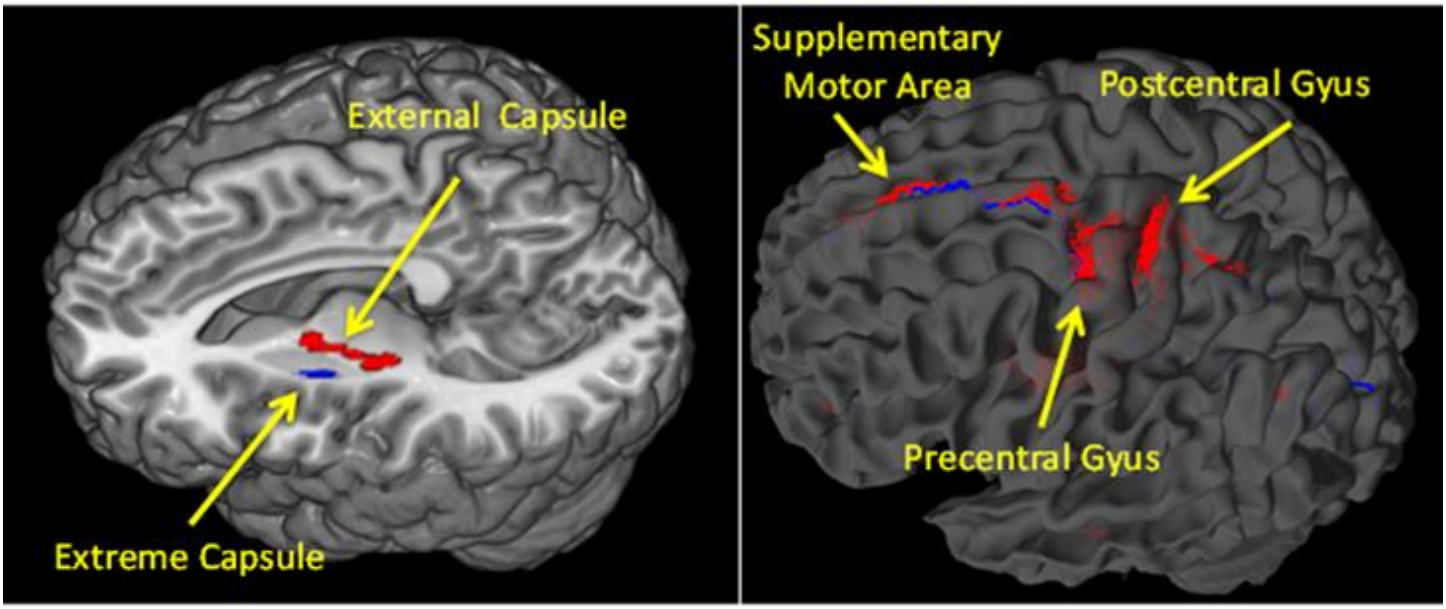

Supplementary Figure 1. Diffusion data. (a) Locations of the reduced MD in the putamen and external capsule for the learning group (blue) and in the internal capsule in the control group (red). (b) Distribution of premotor, supplementary motor, and somatosensory, and motor hand area endpoints of estimated tractography fibers seeded from regions in a.

a

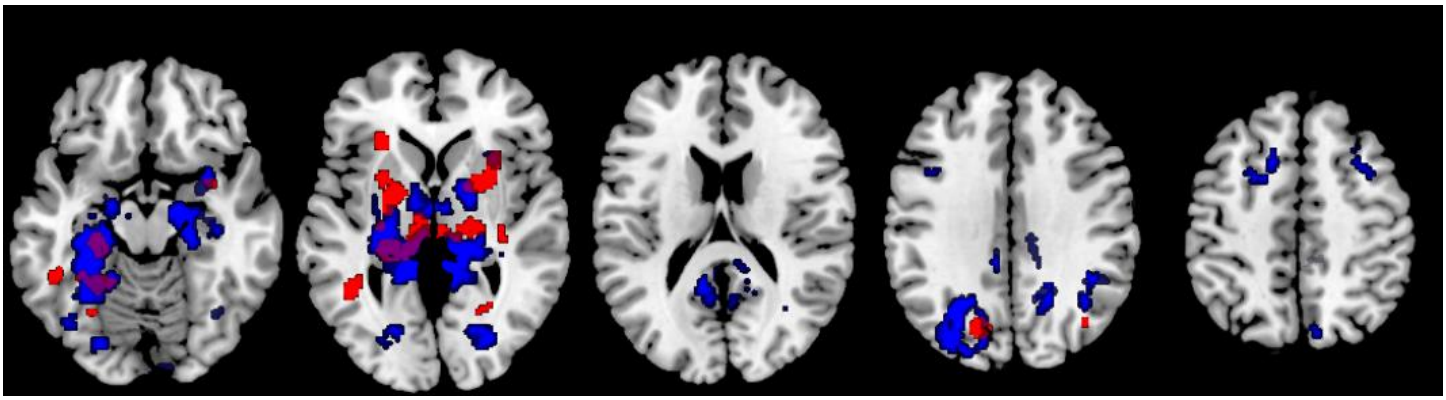

b

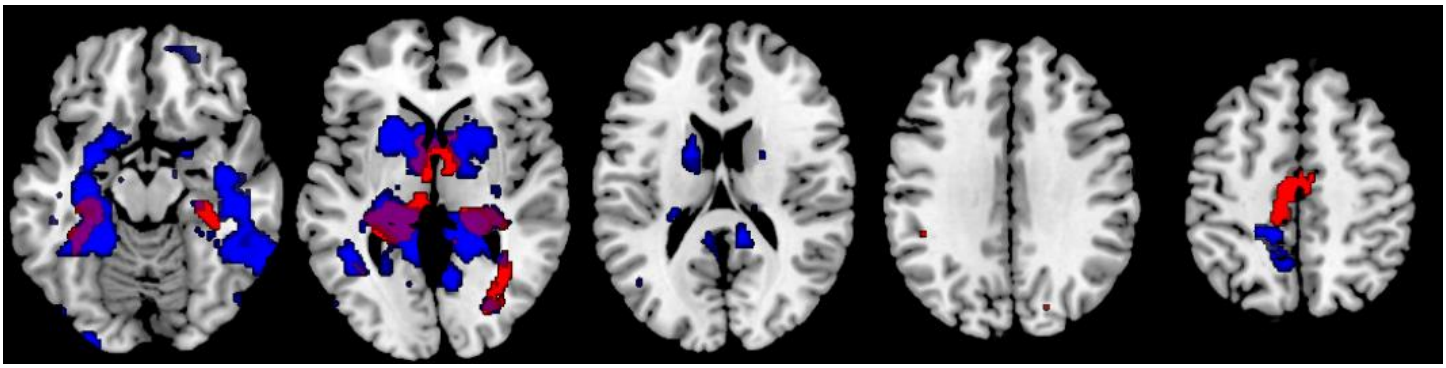

Supplementary Figure 2. Voxel-based analyses of intrinsic functional connectivity with the left hippocampal area of diffusivity decrease as the seed region. Colored voxels show reliable intrinsic synchronization with left hippocampus thresholded at $P < .001$, family-wise error corrected for multiple comparisons. (a) Before training the learning group (blue) and the control group (red) showed parietal connectivity with the hippocampal seed region. (b) Following training, this hippocampal-cortical connectivity was no longer detected at this threshold in either group. At the post-training fMRI scan, the spatial-learning group showed reliable connectivity between the hippocampus and precuneus, and the sensory-motor control group showed reliable connectivity between the hippocampus and left precentral motor areas (right most image). In addition the learning group showed more extensive areas of reliable connectivity with the putamen and caudate. Despite these robust hippocampal connectivity effects in both groups and at both time points, no reliable differences were found between scans for either group or between groups for either scan.

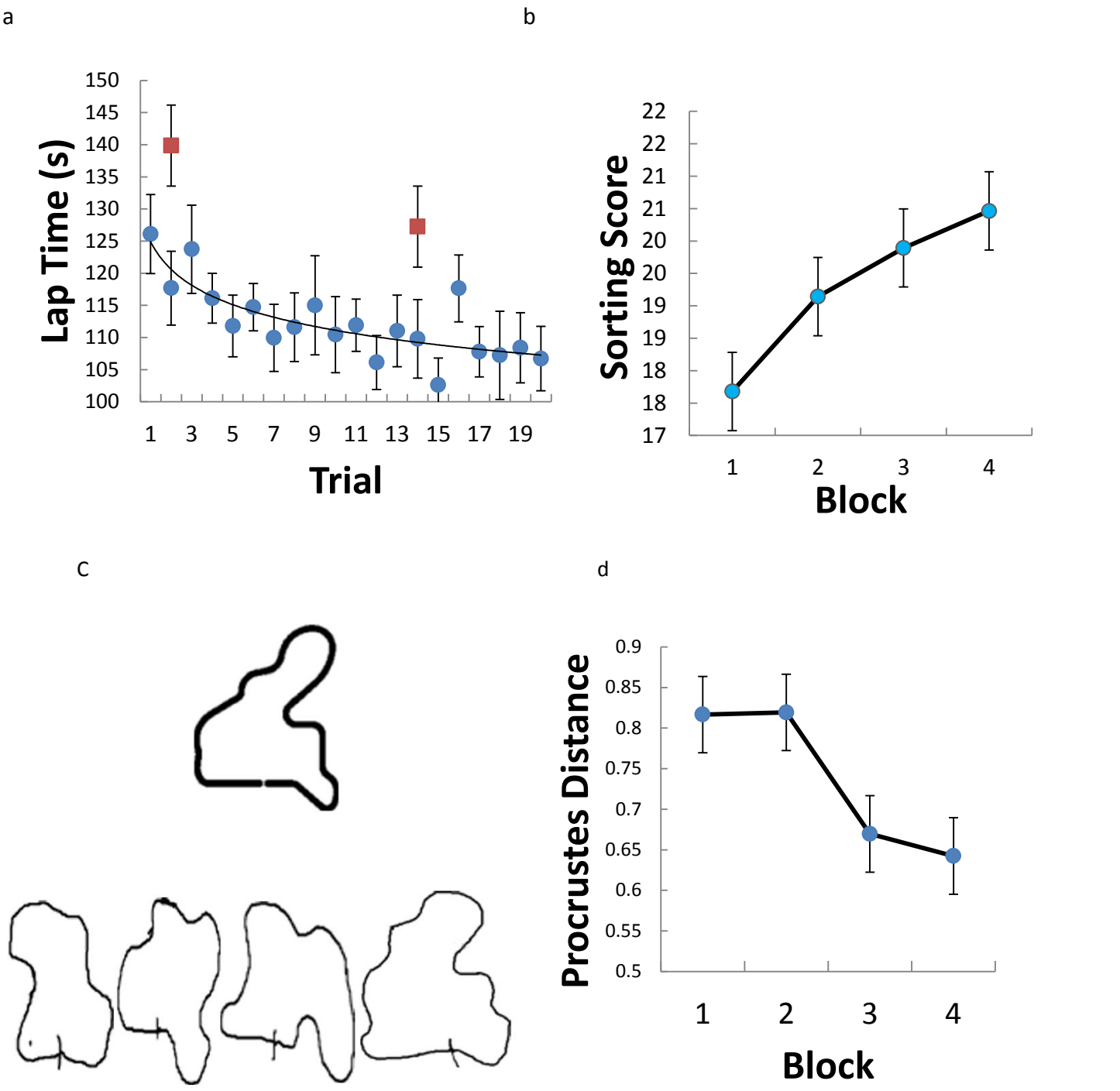

Supplementary Figure 3. Behavioral data. (a) Mean improvement in lap times for the learning group (blue) and for the control group (red) when driving the exact same route. (b) Mean improvement in scores on the sorting task. (c) The true layout of the learned route (top) and an example of one route-learning group participant's sketches of their mental map of the course during training (bottom). (d) The average Procrustes distance between the sketches and the true route decreased over the course of training. Error bars represent the standard error of the mean.

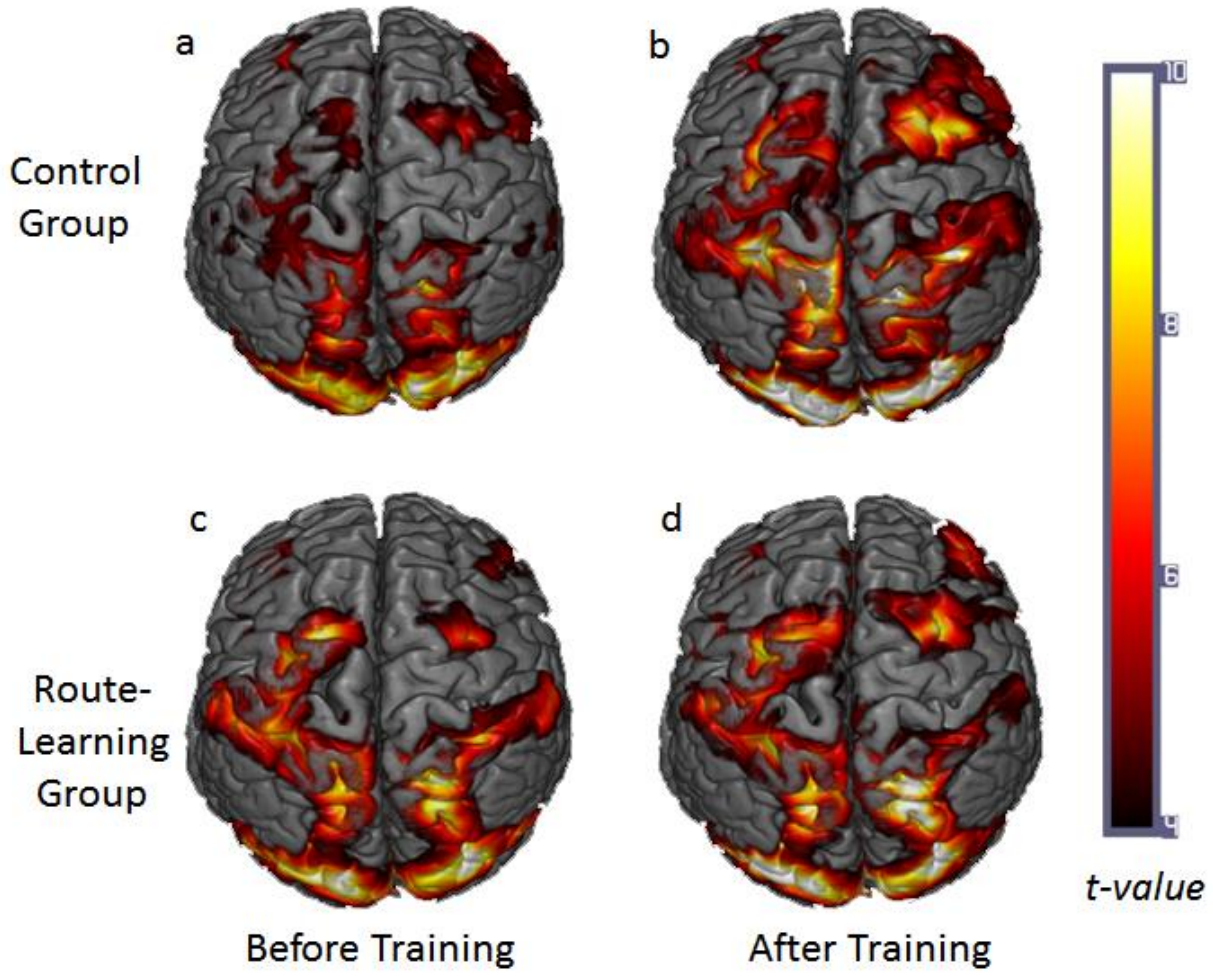

Supplementary Figure 4. Functional magnetic resonance imaging results. Group statistic maps showing reliable differences for the contrast of blood oxygenation level dependent (BOLD) fMRI-measured activation for the simulated driving blocks vs. the resting fixation blocks ($P < .05$, corrected for all voxels in the brain using random field theory). The activation was found in the large scale network previously shown to be involved in such driving tasks, but showed very little change with learning. (a) Control group activation before training. (b) Control group activation following driving practice on different routes. (c) Learning group activation before training. (d) Learning group activation following repeated practice on the same route. There were no reliable effects of either group or time, nor was there an interaction, for the BOLD activation data.